Faculty Publications - Biomedical, Mechanical, and Civil Engineering

Department of Biomedical, Mechanical, and Civil Engineering

2011

Terminal Guidance of Autonomous Parafoils in High Wind-to-Airspeed Ratios

Nathan Slegers
George Fox University, nslegers@georgefox.edu

O A. Yakimenko
Naval Postgraduate School

Follow this and additional works at: https://digitalcommons.georgefox.edu/mece_fac

Part of the Aeronautical Vehicles Commons, and the Navigation, Guidance, Control and Dynamics Commons

Terminal guidance of autonomous parafoils in high wind-to-airspeed ratios

N Slegers[1]* and **O A Yakimenko**[2]

[1]Department of Mechanical and Aerospace Engineering, University of Alabama in Huntsville, Huntsville, Alabama, USA

[2]Department of Mechanical and Astronautical Engineering, Naval Postgraduate School, Monterey, California, USA

Abstract: Autonomous precision placement of parafoils is challenging because of their limited control authority and sensitivity to winds. In particular, when wind speed is near the airspeed, guidance is further complicated by the parafoils inability to penetrate the wind. This article specifically addresses the terminal phase and develops an approach for generating optimal trajectories in real-time based on the inverse dynamics in the virtual domain. The method results in efficient solution of a two-point boundary-value problem using only a single optimization parameter allowing the trajectory to be generated at a high rate, mitigating effects of the unknown winds. It is shown through simulation and experimental results that the proposed algorithm works well even in strong winds and is robust to sensor errors and wind uncertainty.

Keywords: optimal control, parafoils, predictive control, trajectory optimization

1 INTRODUCTION

Precision payload delivery using guided parafoils has extended military re-supply capability by providing accurate and rapid response at substantial offsets with a minimal risk to the cargo delivery aircraft. Significant efforts have been underway to improve precision airdrop with the US Department of Defense's Joint Precision Airdrop System (JPADS) programmes [**1**] being an example. The JPADS self-guided programmes are separated into five classes according to size: micro light weight (MLW) 4–70 kg, ultra light weight (ULW), 100–320 kg, extra light (XL) 320–1000 kg, light (L) 2200–4500 kg, and medium (M) 6800–14 000 kg [**2**]. Most existing efforts have focused on larger systems above 200 kg including; Onyx from Atair Aerospace, Panther from Pioneer Aerospace, Screamer from Strong Enterprises, and Spades from Dutch Space all demonstrated at the Precision Airdrop Technology Conference and Demonstration in 2007 [**3**]. Recently, there has been a new focus on smaller systems with the start of the Joint Medical Distance Support & Evacuation (JMDSE)

programme in 2009. The JMDSE programme is focused on small medical equipment delivery in the MLW and ULW classes and the integration into small unmanned autonomous systems.

Autonomous parafoils for precision delivery are unique aerospace systems with challenges including limited control authority and sensitivity to winds. Parafoils typically only have lateral control using asymmetric brake deflection, with longitudinal control using symmetric deflection being very limited. The absence of thrust, combined with low airspeed, makes wind a significant contributor to a parafoil's trajectory. Airspeed for parafoils can range from 6 m/s for very small lightly loaded systems to over 20 m/s for larger systems. This results in the common occurrence for parafoils where the wind speed may be near or exceed the airspeed. In the case where wind speed exceeds airspeed, the parafoil cannot advance towards the target if the target is upwind. This becomes increasingly likely for parafoils in the MLW class.

Guidance strategies for parafoils vary significantly over the spectrum of systems; however, there are some common aspects seen in all systems. One common aspect is the parafoil is released upwind of the target at a sufficient altitude to ensure that the target can be reached. In addition, all strategies have some combination of homing and energy management phases followed by terminal guidance. Homing refers to the

Corresponding author: Department of Mechanical and Aerospace Engineering, University of Alabama in Huntsville, Technology Hall, Huntsville, Alabama 35899, USA.

email: slegers@mae.uah.edu

process of bringing the system from one region to another region while energy management refers to loitering in a pattern allowing the system to reach an altitude where the parafoil can proceed to impact the target. Assuming homing and energy management stages bring the parafoil to a location where arriving at the target in the presence of wind is possible, the terminal guidance algorithm determines the final accuracy. Homing and energy management are necessary, but not critical, in determining final accuracy because it is relatively easy to bring the system to the target, but quite difficult to plan terminal guidance to co-ordinate arriving at the target and ground simultaneously.

Examples of simple strategies are Onyx by Atair Aerospace [**3**, **4**] and Screamer by Strong Enterprises [**3**] where homing takes the system to the target, energy management is a spiral around the target at a varying radius, followed by terminal guidance as a straight path near the ground. In theory, this simple strategy limits the error to the spiral radius. However, in practice the strategy is limited to the case where wind speed is significantly less than airspeed in order to remain over the target and maintain guidance stability [**5**] making it unsuitable for high wind-to-airspeed ratios. Another limitation of the spiraling strategy is that it cannot guarantee landing into the wind, which is preferred because it minimizes speed at impact. Several other types of guidance concepts for parafoils have also been developed, including optimal control, trajectory databases, model predictive control, and direct glide slope control [**6–10**]. More recently, terminal guidance strategies using optimal trajectories have been investigated. Carter *et al.* developed a method for generating bandwidth limited optimal terminal guidance trajectories [**11**]. Limiting the trajectory bandwidth results in trajectories that are easily tracked. The trajectory was parameterized using five parameters with the optimization problem iteratively solved to minimize final position and heading error. Rademacher *et al.* [**12**] proposed a hybrid approach where optimal trajectories were found using either modified Dubins paths or minimum control trajectories with multiple optimization parameters. The hybrid strategy was employed, because each method had different initial conditions where numerical robustness was a problem or non-existence of solutions existed. In both references [**11**] and [**12**], kinematic parafoil models were used and the optimal trajectories were tracked using proportional-integral-derivative (PID) controllers.

This article develops an optimal terminal guidance algorithm that is robust in high winds even if the wind speed exceeds the parafoil's airspeed. An optimal terminal trajectory is found using a kinematic model similar to references [**11**] and [**12**]. However, using the direct method of calculus of variations and inverse dynamics in a virtual domain, the problem is reduced to a single parameter optimization problem

[**13**]. The result is an extremely efficient solution that is easily solved in real-time. In addition, since the entire terminal trajectory is solved, a model predictive controller (MPC) [**8**] is used to track the trajectory rather than a PID algorithm. A complete six degrees-of-freedom (DoF) model is used to evaluate the method in simulation and demonstrate its application including parafoil turning dynamics. Finally, experimental results are shown where the algorithm was used on a small 2.3 kg parafoil.

2 GUIDANCE STRATEGY

In order to ensure the parafoil system can reach a desired target it is released upwind of a target at high altitudes. The result is typical parafoil precision placement algorithms having an energy management and homing region. The proposed strategy for precision placement shown in Fig. 1 is divided into four phases with the first being energy management, the second homing, followed by terminal guidance comprising a final turn and final approach (FA). Guidance geometry is defined by the target location and four parameters: an away distance, cycle distance, turn diameter, and wind heading angle.

Energy management is commenced after the system is released. The parafoil travels clockwise around the rectangular region defined by the away distance, cycle distance, and turn diameter. The away distance is selected so that in the case of wind speed exceeding airspeed the parafoil will still be able to reach the target, while in energy management, the parafoil continually estimates descent rate and wind speed. Descent rate and wind speed estimates, combined with a distance from the target, are used to determine an altitude z_{start} where energy management is terminated and homing commences. In the homing phase
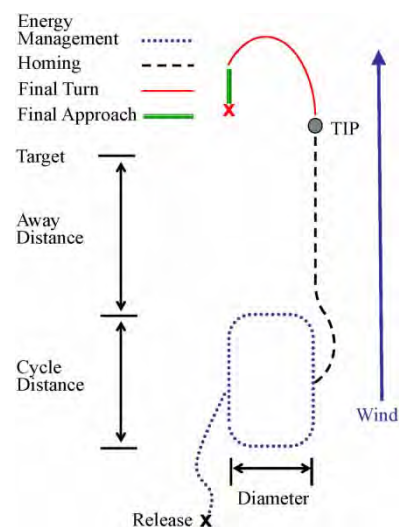

Fig. 1 Guidance strategy

the system travels toward the target while continuing to estimate wind and vertical velocity. All estimated data are used to determine a turn initiation point (TIP) at a distance D_{switch} downwind of the target where terminal guidance will begin. Terminal guidance starts with a final turn followed by an FA into the wind.

3 TERMINAL GUIDANCE

Development of energy management and homing strategies is flexible with the only requirement being that the parafoil is brought near the TIP with sufficient altitude. In contrast, terminal guidance is the most critical stage of parafoil precision placement with a very strict time limitation. The parafoil can be slightly late or earlier departing to and arriving at all other phases, but terminal guidance ends sharply at landing requiring special precautions to be made in building a control algorithm. An ideal terminal guidance trajectory is described in Fig. 2 where, i_I, and j_I, are axes of the standard North–East–Down inertial reference frame, and i_T, and j_T are target axes aligned with the wind W. The parafoil is a distance L upwind of the target, t_{start} is the current time, and R is the final turn radius.

The final turn is initiated at the TIP, occurring at time t_0, a distance D_{switch} past the target. After the TIP is reached the final turn is defined by a commanded yaw $\psi(t)$ occurring from time t_0 until the FA is reached at time t_1. The resulting final turn time is then $T_{\text{turn}} = t_1 - t_0$. The desired FA time T_{app} is $t_2 - t_1$ where t_2 is at touchdown. Transition from the final turn to the FA occurs at t_{exit}.

In terminal guidance described above, the target location R, and a desired T_{app} are specified, while the wind W is estimated online and the altitude z and L are measured. The terminal guidance problem can then be summarized as follows. For a parafoil in the pres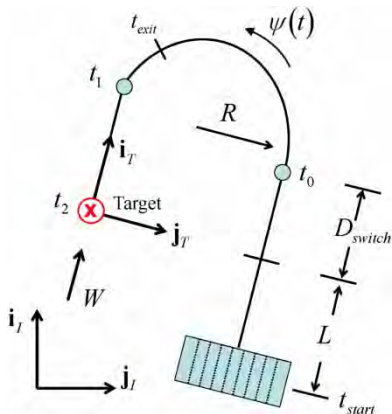ence of wind W, at altitude z, and a distance L from the target, find the distance D_{switch} to the final TIP for an ideal impact at t_2.

In general, the dynamic model of a parafoil is complex and non-linear, so that the problem can only be solved numerically. However, some assumptions can be made, allowing an analytical solution to be used as a reference trajectory. These assumptions are a slow turn rate, so that the roll and sideslip angles can be ignored, and nearly constant descent rate V_ν and horizontal airspeed V_{h}. In this case it immediately follows that

$$t_2 = t_{\text{start}} - \frac{z_{\text{start}}}{V_{\text{v}}} \tag{1}$$

The problem reduces to a kinematic model represented by three components of the ground velocity in the target axes

$$\begin{bmatrix} \dot{x} \\ \dot{y} \\ \dot{z} \end{bmatrix} = \begin{bmatrix} -W + V_{\text{h}}\cos\psi \\ V_{\text{h}}\sin\psi \\ V_{\text{v}} \end{bmatrix} \tag{2}$$

where x, y, and z are positions in the target frame. Now, the commanded turn $\psi(t)$ can be chosen as any function that satisfies the boundary conditions $\psi(t_0) = 0$ and $\psi(t_1) = -\pi$ with respect to the wind while satisfying the constraint that the distance travelled in j_T is $-2R$. For a constant turn rate, the solution to the final turn time T_{turn} and turn rate are

$$\dot{\psi} = -\frac{V_{\text{h}}}{R} \tag{3}$$

$$T_{\text{turn}} = \frac{\pi R}{V_{\text{h}}} \tag{4}$$

Hence, the most straightforward algorithm to control the final turn, is to track the turn rate $-V_{\text{h}}/R$. Assuming that the wind W is constant and using the commanded turn rate $\dot{\psi}^c = -V_{\text{h}}/R$, integration of inertial velocities along i_T and j_T from t_{start} to t_2 yield

$$D_{\text{switch}} + \int_{t_0}^{t_1} \dot{x}\,dt + \int_{t_1}^{t_2} \dot{x}\,dt$$
$$= D_{\text{switch}} - WT_{\text{turn}} - (V_{\text{h}} + W)T_{\text{app}} = 0 \tag{5}$$

$$z + V_{\text{v}}\left(\frac{L + D_{\text{switch}}}{V_{\text{h}} - W}\right) + V_{\text{v}}T_{\text{turn}} + V_{\text{v}}T_{\text{app}} = 0 \tag{6}$$

Equations (5) and (6) can then be solved for D_{switch} and T_{app} resulting in

$$D_{\text{switch}} = WT_{\text{turn}} + \left(\frac{V_{\text{h}}^2 - W^2}{2V_{\text{h}}}\right)$$
$$\times \left(\frac{-z}{V_{\text{v}}} - T_{\text{turn}} - \frac{L + WT_{\text{turn}}}{V_{\text{h}} - W}\right) \tag{7}$$

$$T_{\text{app}} = \left(\frac{V_{\text{h}} - W}{2V_{\text{h}}}\right)\left(\frac{-z}{V_{\text{v}}} - T_{\text{turn}}\right) - \frac{L + WT_{\text{turn}}}{2V_{\text{h}}} \tag{8}$$

From equations (7) and (8) it can be seen that the higher the altitude z, the larger D_{switch} and T_{app} become.

Fig. 2 Terminal guidance manoeuver
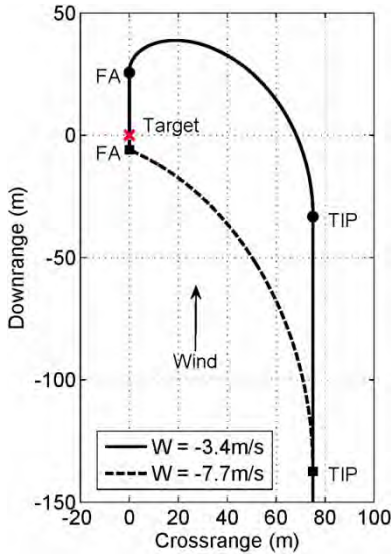
Fig. 3 Simulated guidance in ideal conditions (● TIP and FA $W = -3.4$ m/s, ■ TIP and FA $W = -7.7$ m/s)

Fig. 4 Final turn trajectories with initial condition errors

As the parafoil loiters upwind of the target, z_{start} the altitude at which to turn towards the target can be found using a desired FA time $T_{\text{app}}^{\text{des}}$. The switching altitude to exit energy management which achieves $T_{\text{app}}^{\text{des}}$ is then given by solving equation (8) for z, resulting in

$$z_{\text{start}} = -V_{\text{v}} \left(T_{\text{turn}} + \frac{L + WT_{\text{turn}}}{V_{\text{h}} - W} + \frac{2V_{\text{h}}}{V_{\text{h}} - W} T_{\text{app}}^{\text{des}} \right) \quad (9)$$

Once the system is homing towards the target the goal is to bring the system to the point defined by $x = D_{\text{switch}}$ and $y = -2R$ with D_{switch} continually estimated during homing using equation (7) and current estimates of V_{h}, V_{v}, and W. A desired FA time $T_{\text{app}}^{\text{des}}$ is used in equation (9) in making the decision to exit energy management. However, disturbances, measurement error, and tracking error while homing will alter the ideal terminal guidance resulting in an actual T_{app} being estimated during homing using equation (7).

Figure 3 demonstrates trajectories starting 150 m upwind of the target when there are no disturbances and the commanded yaw rate is tracked precisely for a horizontal airspeed of 6.82 m/s, descent rate of 3.05 m/s, turn radius of 37.5 m, and a desired FA time $T_{\text{app}}^{\text{des}}$ of 7.5 s. Trajectories for two wind magnitudes are shown, −3.4 and 7.7 m/s, resulting in the wind speed being 50 per cent and 110 per cent of the airspeed. The manoeuvre in winds of 50 per cent of the airspeed starts at an altitude of 110 m resulting in the TIP at a distance D_{switch} of −33.3 m and the FA beginning 25.7 m downwind of the target. In contrast, when the wind speed is 110 per cent of the airspeed the manoeuver starts at an altitude of 78 m with the TIP at a distance D_{switch} of −137 m and the FA beginning 6.0 m upwind of the target, with the parafoil travelling backwards at impact.
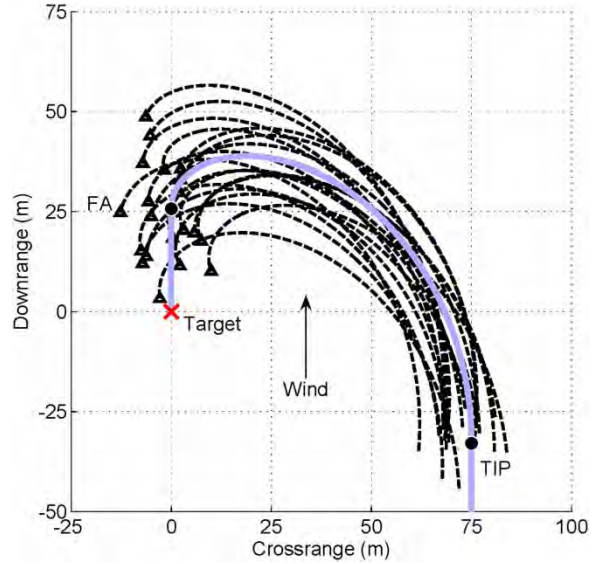
In practice, sensor errors, uncertain winds, and imperfect control will disturb the ideal touchdown depicted above. Figure 4 shows Monte Carlo simulations with $W = -3.4$ m/s, where it is assumed error in the initial horizontal position, heading, and wind occur at the beginning of terminal guidance. The standard deviation was assumed to be 6 m in each co-ordinate, $10°$ in heading, and 0.5 m/s in wind speed. As seen from Fig. 4, these errors result in spreading the arrival to the FA point. Therefore, while the simplified algorithm may provide a reasonable strategy for exiting the energy management phase, an effective terminal guidance strategy must compensate for sensor errors and varying winds during the final turn.

4 OPTIMAL TERMINAL GUIDANCE

To overcome tracking errors and unaccounted winds, the following two-point boundary-value problem (TPBVP) is formulated. Staring at $t = 0$ with the state vector defined as $\boldsymbol{x}_0 = [x_0, y_0, \psi_0]^{\text{T}}$, the system influenced by the last known wind needs to be brought to another point, $\boldsymbol{x}_f = [(V_{\text{h}} + W) T_{\text{app}}^{\text{des}}, 0, -\pi]^{\text{T}}$ at $t = t_f$. Hence, they need to find the trajectory that satisfies these boundary conditions along with a constraint imposed on yaw rate, $|\dot{\psi}| \leqslant \dot{\psi}_{\text{max}}$, while finishing the manoeuver in exactly T_{turn} seconds. The optimal $\psi(t)$ is then tracked by the guidance unit using any appropriate control algorithm. Errors and unaccounted winds will not allow exact tracking of the calculated optimal trajectory; therefore, computation of an optimal trajectory will be updated during the final turn, each time starting from the current state, requiring the system to arrive at $\boldsymbol{x}_f = [(V_{\text{h}} + W) T_{\text{app}}^{\text{des}}, 0, -\pi]^{\text{T}}$ in T_{turn} seconds from the beginning of the turn. The remaining time

until arrival at the FA is computed as

$$t_f = -\frac{z}{V_v} - T_{app}^{final} \tag{10}$$

where T_{app}^{final} is the final calculated approach time from equation (8) before entering the final turn.

Development of the optimal trajectory algorithm begins by recalling from equation (2) the target frame horizontal trajectory kinematics

$$\begin{bmatrix} \dot{x} \\ \dot{y} \end{bmatrix} = \begin{bmatrix} -W + V_h \cos\psi \\ V_h \sin\psi \end{bmatrix} \tag{11}$$

Recognizing that if the final turn horizontal trajectory is given by equation (11) the yaw angle along this trajectory is related to the change of inertial co-ordinates as

$$\psi = \tan^{-1}\frac{\dot{y}}{\dot{x} + W} \tag{12}$$

Differentiating equation (12) provides the yaw rate control

$$\dot{\psi} = \frac{\ddot{y}(\dot{x} + W) - \ddot{x}\dot{y}}{(\dot{x} + W)^2 + \dot{y}^2} \tag{13}$$

required to follow the reference final turn trajectory in presence of constant wind W. The inertial speed along the trajectory will also depend on the current yaw angle

$$V_G = \sqrt{\dot{x}^2 + \dot{y}^2} = \sqrt{V_h^2 + W^2 - 2V_hW\cos\psi} \tag{14}$$

Now, following the general idea of direct methods of calculus of variations [**13**] the solution of the TPBVP will be represented as functions of some scaled argument $\bar{\tau} = \tau/\tau_f \in [0;1]$

$$
\begin{aligned}
x(\bar{\tau}) = P_1(\bar{\tau}) &= a_0^1 + a_1^1\bar{\tau} + a_2^1\bar{\tau}^2 + a_3^1\bar{\tau}^3 \\
&\quad + b_1^1\sin(\pi\bar{\tau}) + b_2^1\sin(2\pi\bar{\tau}) \\
y(\bar{\tau}) = P_2(\bar{\tau}) &= a_0^2 + a_1^2\bar{\tau} + a_2^2\bar{\tau}^2 + a_3^2\bar{\tau}^3 \\
&\quad + b_1^2\sin(\pi\bar{\tau}) + b_2^2\sin(2\pi\bar{\tau})
\end{aligned} \tag{15}
$$

Coefficients a_i^η and b_i^η $(\eta = 1,2)$ are defined by the boundary conditions up to the second-order derivative at $\tau = 0$ and $\tau = \tau_f$ ($\bar{\tau} = 1$). According to the problem formulation and equation (11), these boundary conditions are

$$
\begin{bmatrix} x \\ y \end{bmatrix}_{\tau=0} = \begin{bmatrix} x_0 \\ y_0 \end{bmatrix}, \quad \begin{bmatrix} \dot{x} \\ \dot{y} \end{bmatrix}_{\tau=0} = \begin{bmatrix} -W + V_h\cos\psi_0 \\ V_h\sin\psi_0 \end{bmatrix},
$$
$$
\begin{bmatrix} \ddot{x} \\ \ddot{y} \end{bmatrix}_{\tau=0} = \begin{bmatrix} -\dot{\psi}_0 V_h\sin\psi_0 \\ \dot{\psi}_0 V_h\cos\psi_0 \end{bmatrix} \tag{16}
$$

$$
\begin{bmatrix} x \\ y \end{bmatrix}_{\tau=\tau_f} = \begin{bmatrix} (V_h + W)T_{app}^{des} \\ 0 \end{bmatrix},
$$
$$
\begin{bmatrix} \dot{x} \\ \dot{y} \end{bmatrix}_{\tau=\tau_f} = \begin{bmatrix} -W - V_h \\ 0 \end{bmatrix}, \quad \begin{bmatrix} \ddot{x} \\ \ddot{y} \end{bmatrix}_{\tau=\tau_f} = \begin{bmatrix} 0 \\ 0 \end{bmatrix} \tag{17}
$$

While final condition equation (17) will be constant, initial conditions will reflect the current state of the system at each cycle of optimization. Differentiation of equation (15) two times with respect to τ results in

$$
\begin{aligned}
\tau_f P_\eta'(\bar{\tau}) &= a_1^\eta + 2a_2^\eta\bar{\tau} + 3a_3^\eta\bar{\tau}^2 + \pi b_1^\eta\cos(\pi\bar{\tau}) \\
&\quad + 2\pi b_2^\eta\cos(2\pi\bar{\tau}) \\
\tau_f^2 P_\eta''(\bar{\tau}) &= 2a_2^\eta + 6a_3^\eta\bar{\tau} - \pi^2 b_1^\eta\sin(\pi\bar{\tau}) \\
&\quad - (2\pi)^2 b_2^\eta\sin(2\pi\bar{\tau})
\end{aligned} \tag{18}
$$

Equating equation (18) at the terminal point to the known boundary conditions equations (16) and (17) yields a system of linear algebraic equations for coefficients a_i^η and $(b_i^\eta \eta = 1,2)$. For instance, in the x-co-ordinate

$$
\begin{bmatrix}
1 & 0 & 0 & 0 & 0 & 0 \\
1 & 1 & 1 & 1 & 0 & 0 \\
0 & 1 & 0 & 0 & \pi & 2\pi \\
0 & 1 & 2 & 3 & -\pi & 2\pi \\
0 & 0 & 2 & 0 & 0 & 0 \\
0 & 0 & 2 & 6 & 0 & 0
\end{bmatrix}
\begin{bmatrix}
a_0^1 \\ a_1^1 \\ a_2^1 \\ a_3^1 \\ b_1^1 \\ b_2^1
\end{bmatrix}
=
\begin{bmatrix}
x_0 \\ x_f \\ x_0'\tau_f \\ x_f'\tau_f \\ x_0''\tau_f^2 \\ x_f''\tau_f^2
\end{bmatrix} \tag{19}
$$

Resolving equation (19) yields

$$
\begin{aligned}
a_0^1 &= x_0, \quad a_1^1 = -(x_0 - x_f) + \frac{(2x_0'' + x_f'')\tau_f^2}{6}, \\
a_2^1 &= \frac{x_0''\tau_f^2}{2}, \quad a_3^1 = -\frac{(x_0'' - x_f'')\tau_f^2}{6} \\
b_1^1 &= \frac{2(x_0' - x_f')\tau_f + (x_0'' + x_f'')\tau_f^2}{4\pi} \\
b_2^1 &= \frac{12(x_0 - x_f) + 6(x_0' + x_f')\tau_f + (x_0'' - x_f'')\tau_f^2}{24\pi}
\end{aligned} \tag{20}
$$

The only problem is that derivatives in equation (20) are taken in the virtual domain, while the actual boundary conditions are given in the physical domain. Mapping between the virtual domain $[0;\tau_f]$ and physical domain $[0;t_f]$ is addressed by introducing a speed factor λ

$$\lambda = \frac{d\tau}{dt} \tag{21}$$

Using this speed factor the authors may now compute corresponding derivatives in the virtual

domain using the differentiation rules valid for any time-variant parameter ξ

$$\dot{\xi} = \lambda\xi', \quad \ddot{\xi} = \lambda(\lambda'\xi' + \lambda\xi'') \qquad (22)$$

Inverting equation (22) yields

$$\xi' = \lambda^{-1}\dot{\xi}, \quad \xi'' = \lambda^{-2}\ddot{\xi} - \lambda'\lambda^{-1}\dot{\xi} \qquad (23)$$

needed to transfer the boundary conditions. The speed factor λ simply scales the entire problem – the higher speed factor λ is, the larger τ_f it results in reference [14] – one may let $\lambda = 1$ and $\lambda' = 0$ at the boundary conditions which means one can safely assume at the boundary conditions $\xi' = \dot{\xi}$ and $\xi'' = \ddot{\xi}$.

Finding the optimal solution among all candidate trajectories described by equation (15) begins by first guessing a value of the only varied parameter τ_f. For the initial value of τ_f one can take the length of the circumference connecting terminal points as

$$\tau_f = \frac{\pi}{2}\sqrt{(x_f - x_0)^2 + (y_f - y_0)^2} \qquad (24)$$

Coefficients of the candidate trajectory are computed using equation (20) with the boundary conditions equations (16) and (17) converted to the virtual domain. Having an analytical representation of the candidate trajectory equations (15) and (18) defines the values of x_j, y_j, x_j', and y_j', $j = 1, \ldots, N$ over a fixed set of N points spaced evenly along the virtual arc $[0; \tau_f]$ with the interval

$$\Delta\tau = \tau_f(N-1)^{-1} \qquad (25)$$

so that

$$\tau_j = \tau_{j-1} + \Delta\tau, \quad j = 2, \ldots, N, \quad (\tau_1 = 0) \qquad (26)$$

Next, for each node $j = 2, \ldots, N$ compute

$$\Delta t_{j-1} = \sqrt{\frac{(x_j - x_{j-1})^2 + (y_j - y_{j-1})^2}{V_h^2 + W^2 - 2V_h^W \cos\psi_{j-1}}} \qquad (27)$$

$(\psi_1 \equiv \psi_0)$, and

$$\lambda_j = \Delta\tau \Delta t_{j-1}^{-1} \qquad (28)$$

The yaw angle ψ can now be computed using the virtual domain version of equation (12)

$$\psi_j = \tan^{-1}\frac{\lambda_j y_j'}{\lambda_j x_j' + W} \qquad (29)$$

Finally, the yaw rate $\dot{\psi}$ is evaluated simply as

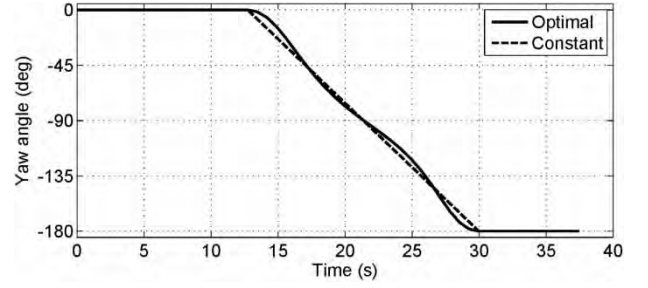$$\dot{\psi}_j = (\psi_j - \psi_{j-1})\Delta t_{j-1}^{-1} \qquad (30)$$

Fig. 5 Comparison of optimal and constant turn rate

When all parameters are computed at each of the N points, one can compute the performance index

$$J = \left(\sum_{j=1}^{N-1}\Delta t_j - T_{\text{turn}}\right)^2 + k^{\dot{\psi}}\Delta \qquad (31)$$

where

$$\Delta = \max_j \left(0; \left|\dot{\psi}_j\right| - \dot{\psi}_{j\max}\right)^2 \qquad (32)$$

with $k^{\dot{\psi}}$ being a weighting coefficient.

The optimal trajectory problem based on the direct method has now been turned into a single-parameter optimization problem where τ_f is found such that equation (31) is minimized subject to the system in equations (2) and (11). The problem is solved using a non-gradient optimization numerical algorithm based on the golden section search and parabolic interpolation method [15]. Reduction of finding an optimal terminal trajectory to a single-parameter optimization results in short computation times. To be more specific, a 16-bit 80 MHz microprocessor allowed computation of a 17.5 s turn manoeuver with $N = 25$ in ten iterations, in only 0.07 s.

As a demonstration of the proposed approach, Fig. 5 shows an example of the optimal final turn for the case in Fig. 3 when $W = -3.4$ m/s. The optimal final turn and constant turn rate commands are similar; however, as opposed to the constant turn rate, the yaw angle changes smoothly at departure from the TIP and arrival at the FA. As a result, the optimal turn trajectory is slightly different but, more importantly, the system still captures the FA in exactly T_{turn} seconds. Therefore, the authors have a tool allowing construction of the optimal trajectory from any initial point to the predetermined final. To this end, Fig. 6 shows that using the same initial errors from Fig. 4 the optimal turn is found so that the systems still arrive at the FA in the predetermined time, T_{turn}.

Implementation of the algorithm on actual parafoil systems requires three additional components to make it more robust in practice: compensation for full dynamic motion, wind disturbance mitigation, and terminal trajectory tracking errors. The kinematic
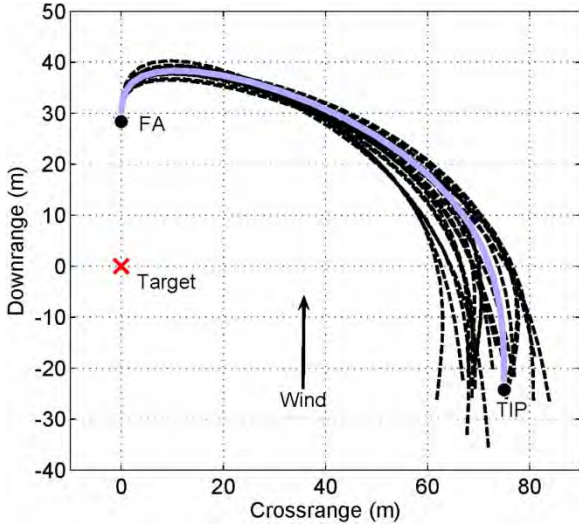
Fig. 6 Optimal guidance with an error in the TIP

model in equation (2) does not account for parafoil turning dynamics and assumes that the sideslip and roll angles are small. When the turn rate is sufficiently small, or the radius R is large, the model in equation (2) provides sufficient accuracy. However, in order to track the desired trajectory for a wide range of R, the error from sideslip and turning dynamics can be compensated by adding an additional commanded ψ^c for the first t_{pre} seconds after the TIP has been reached. Specifically, for the first t_{pre} seconds of the maneuver the command yaw ψ^c produced by equation (29) is augmented as

$$\tilde{\psi}^c = \psi^c - K_{\text{turn}} \frac{V_{\text{h}}}{R} \tag{33}$$

where K_{turn} is the correction gain and V_{h}/R is the required constant turn rate in equation (4). Disturbances from wind and sensor errors during tracking of the optimal trajectory will result in errors in the FA arrival. These errors can be accommodated by updating the optimal trajectory from the current conditions to the desired FA point during the final turn. Re-computation of the optimal trajectory is scheduled so that a specified number of updates occur at equal intervals over the period from t_0 to t_{exit}. Finally, the FA location, x_f in equation (17), assumes that during the FA the parafoil travels directly to the target by the shortest path. In practice, disturbances and the guidance algorithm results in a trajectory with less than perfect efficiency at reaching the target. In order to correct for realistic errors during the FA the location x_f is corrected to be

$$x_f = V_{\text{h}} T_{\text{app}}^{\text{des}} \varepsilon_{\text{final}} \tag{34}$$

where $\varepsilon_{\text{final}}$ is the FA efficiency.

5 PRECISION PLACEMENT SIMULATION

In the previous development of an optimal terminal trajectory a kinematic model was used and it was assumed the trajectory was tracked perfectly. However, actual parafoil systems have turning dynamics resulting in side slip and varying descent rates. Evaluation of the proposed algorithm will be done using a higher fidelity model. The combined parafoil canopy and payload can be modelled using six DoF, which include three inertial position components of the system mass centre as well as the three Euler orientation angles of the parafoil–payload system, yaw ψ, pitch θ, and roll φ. The 6 DoF model described in reference [9] is used in all simulations with a constant canopy incidence angle Γ, payload drag included in the system aerodynamic coefficients, and the canopy apparent mass approximated by assuming the canopy has two axes of symmetry.

The guidance strategy outlined in sections 2 to 4 requires a controller that tracks a commanded yaw ψ^c, using the brake deflection δ_a. A simple two DoF model of the roll and yaw dynamics can be used for developing a yaw controller since for parafoils, pitch and speed are not typically controllable. The state vector for the two DoF rotational model is $\boldsymbol{x} = [\phi, \psi, p, r]^{\text{T}}$, where p and r are the parafoil roll and pitch rates. A wide range of trajectory tracking controllers used on UAVs could be used [8, 16], however, MPC is selected since the optimal terminal guidance prescribes a desired ψ^c over the terminal trajectory horizon. The rotational kinematics and dynamics described in reference [9] are non-linear and thus linearized to take advantage of well-developed control techniques for linear systems. Assuming that the aerodynamic velocity V_a is constant, the non-linear model with parameters listed in Appendix 2 can be numerically linearized resulting in a linear discrete model for the parafoil with sampling period of 0.5 s

$$\begin{bmatrix} \dot{\phi} \\ \dot{\psi} \\ \dot{p} \\ \dot{r} \end{bmatrix}_{k+1} = \begin{bmatrix} 0.962 & 0 & 0.153 & 0.012 \\ 0.0078 & 1 & -0.011 & 0.043 \\ -0.103 & 0 & 0.033 & 0.004 \\ 0.0191 & 0 & -0.0023 & -0.003 \end{bmatrix} \begin{bmatrix} \phi \\ \psi \\ p \\ r \end{bmatrix}_k$$
$$+ \begin{bmatrix} -0.006 \\ 0.0501 \\ -0.0131 \\ 0.1098 \end{bmatrix} \delta_{a;k} \tag{35}$$

For a given desired discrete output vector $\boldsymbol{\psi}^c = [\psi_{k+1}^c, \psi_{k+2}^c, \ldots, \psi_{k+H_p}^c]^{\text{T}}$ that spans the prediction horizon H_p, MPC solves for the discrete optimal control vector $\boldsymbol{U} = [u_k, u_{k+1}, \ldots, u_{k+H_p-1}]^{\text{T}}$ governed by the linear plant $\boldsymbol{x}_{k+1} = \mathbf{A}\boldsymbol{x}_k + \mathbf{B}u_k$ with output $y_k = \mathbf{C}\boldsymbol{x}_k$ [8, 17]. The single-input single-output parafoil model above has the output matrix $\mathbf{C} = [0\ 1\ 0\ 0]$. The discrete linear model can be used to estimate the future state

of the system as

$$\hat{\boldsymbol{\psi}}^{c} = \mathbf{K_{CA}}\boldsymbol{x}_k + \mathbf{K_{CAB}}\boldsymbol{U} \qquad (36)$$

from the current state vector $\boldsymbol{x}_k$, and the control vector $\boldsymbol{U}$, where

$$\mathbf{K_{CA}} = \begin{bmatrix} \mathbf{CA} \\ \mathbf{CA}^2 \\ \vdots \\ \mathbf{CA}^{H_p} \end{bmatrix} \qquad (37)$$

$$\mathbf{K_{CAB}} = \begin{bmatrix} \mathbf{CB} & 0 & 0 & 0 & 0 \\ \mathbf{CAB} & \mathbf{CB} & 0 & 0 & 0 \\ \mathbf{CA}^2\mathbf{B} & \mathbf{CAB} & \mathbf{CB} & 0 & 0 \\ \vdots & \vdots & \vdots & \ddots & 0 \\ \mathbf{CA}^{H_p-1}\mathbf{B} & \cdots & \mathbf{CA}^2\mathbf{B} & \mathbf{CAB} & \mathbf{CB} \end{bmatrix} \qquad (38)$$

In MPC, the optimization problem is cast as a finite-time discrete optimal control problem. To compute the control input at a given time instant, a quadratic cost function is minimized through the selection of the control history over the control horizon. The cost function can be written as

$$J = \left(\boldsymbol{\psi}^c - \hat{\boldsymbol{\psi}}^c\right)^{\mathrm{T}} \mathbf{Q} \left(\boldsymbol{\psi}^c - \hat{\boldsymbol{\psi}}^c\right) + \boldsymbol{U}^{\mathrm{T}}\boldsymbol{R}\boldsymbol{U} \qquad (39)$$

where $\mathbf{Q}$ and $\mathbf{R}$ are symmetric positive semi-definite matrices of size $H_p \times H_p$ that penalize tracking error and control, respectively. The control $\boldsymbol{U}$, which minimizes equation (39), can be found analytically [17] as

$$\boldsymbol{U} = \left(\mathbf{K_{CAB}^T Q K_{CAB}} + \mathbf{R}\right)^{-1} \mathbf{K_{CAB}^T Q} \left(\boldsymbol{\psi}^c - \mathbf{K_{CA}}\boldsymbol{x}_k\right) \qquad (40)$$

Equation (40) contains the optimal control inputs over the entire control horizon. In practice, only the first control is applied and the problem is updated at the next time update.

Implementation of the terminal guidance algorithm requires both determining the optimal terminal trajectory using the method outlined in section 4 and the trajectory tracking controller in equation (40). The first step in the complete terminal guidance algorithm is to use the current measured parafoil position and velocity along with the known FA point to define the boundary conditions to the TPBVP (equations (16), (17) and (34)). Once the TPBVP has been defined, the guidance algorithm must determine the optimal solution among all candidate trajectories equation (15) by initializing the only varied parameter τ_f according to equation (24). The optimal trajectory is found using the single-parameter optimization problem outlined in section 4 (equations (24) to (32)) with a non-gradient optimization numerical algorithm based on the golden section search and parabolic interpolation method [15]. Upon completion of the optimization problem, the desired yaw angle trajectory is known

from equation (29). Finally, the discrete optimal yaw angle can be combined with the correction in equation (33) and used in the proposed MPC algorithm in equation (40) to determine the final control.

6 SIMULATION RESULTS

In all simulations the full non-linear parafoil model is numerically integrated using a fourth-order Runge–Kutta algorithm with time step of 0.05 s. The MPC control algorithm described previously is used to track $\boldsymbol{\psi}^c$. Figures 7 and 8 show examples of the complete terminal guidance strategy for an R of 37.5 m in winds of -3.4 and -7.7 m/s. In both cases T_{app} is 7.5 s, ε_{final} is 0.95, $t_1 - t_{exit}$ is 3.0 s, t_{pre} is 6.0 s, K_{turn} is 1.0, $\dot{\psi}_{j\max}$ is 20 deg/s, and k^{ψ} is 400, with two trajectory updates made during the final turn. Results are shown from the TIP (x_0, y_0, z_0), which are $(-33, 75,$ and -93 m) in
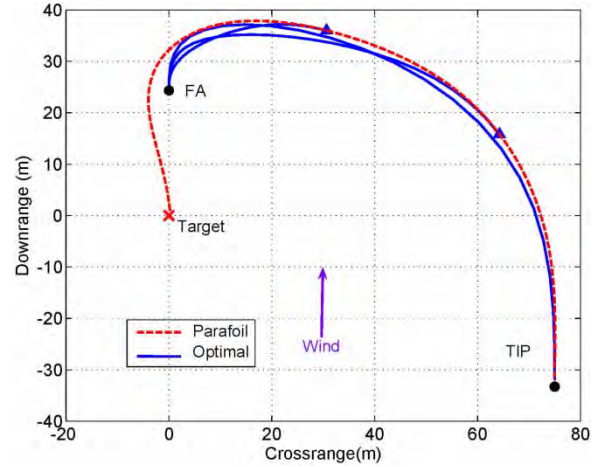

Fig. 7 Optimal real-dynamics-augmented guidance for $W = -3.7$ m/s (▲ trajectory update)

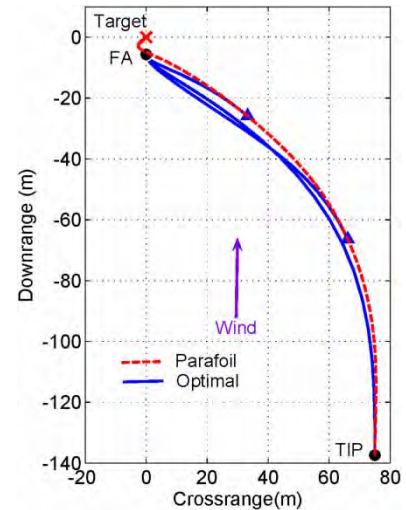**Fig. 8** Optimal real-dynamics-augmented guidance for $W = -7.7$ m/s (▲ trajectory update)

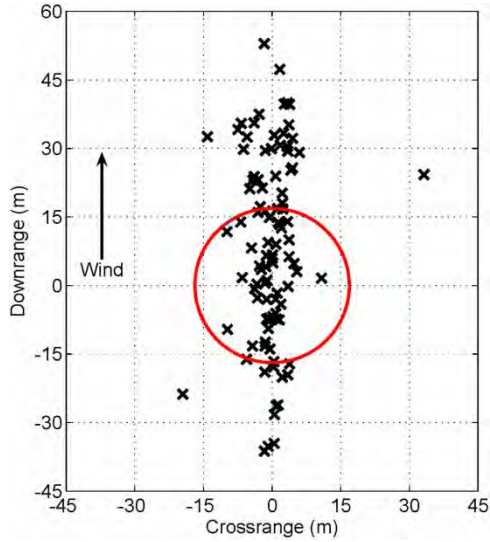**Fig. 9** Monte Carlo simulation dispersion

Fig. 10 Test results of precision placement algorithm

Fig. 8 and ($-137, 75$, and -93 m) in Fig. 9. In both cases the parafoil initially tracks the optimal trajectory; however, errors slowly build due to mismatch in the actual dynamics and the model. At each update a new trajectory is calculated that results in arrival at the FA. Impact errors are 0.4 m in Fig. 7 and 0.5 m in Fig. 8.

The complete precision placement algorithm combines energy management, an exit from energy management based on equation (9), estimation of a TIP during homing using equation (7), and the optimal turn followed by the FA. Monte Carlo simulations of 100 drops were done using the complete precision placement algorithm with an away distance of 450 m, a cycle distance of 125 m, an R of 37.5 m, and the target at the origin. The initial position and altitude were nominally 760 m upwind of the target, at an altitude of 700 m, both normally distributed with a 50 m standard deviation. Gaussian noise was injected into measured position, altitude, and inertial sensors as summarized in Table 1.

In addition to sensor errors, two sources of wind variation were added to the simulation, varying direction and varying ground wind magnitude. Wind is assumed to have a constant magnitude prior to terminal guidance but varies linearly from W at the TIP

Table 1 Error statistics

Parameter	1σ
GPS bias (m)	2.0
GPS noise (m)	0.5
Altitude bias (m)	2.0
Altitude noise (m)	0.5
Roll, pitch, and yaw bias (degree)	2.0
Roll, pitch, and yaw noise (degree)	1.0
u, v, and w bias (m/s)	0.1
u, v, and w noise (m/s)	0.2
p, q, and r bias (degree/s)	1.0
p, q, and r noise (degree/s)	1.0

to $W + W_F$ at the ground. The wind W is normally distributed with 4.75 m/s mean and 2.0 m/s standard deviation while W_F is 1.5 m/s (1σ). For the example parafoil, this results in a nominal wind-to-airspeed ratio of 0.70 with 25 per cent exceeding 1.0. Prevailing wind is assumed by the system to travel down range at a heading of zero degrees while the true wind heading varies $15°(1\sigma)$ in direction. Dispersion results are shown in Fig. 9. The resulting circular error probable (CEP) shown by the circle is 16.8 m and is defined by the radius which includes 50 per cent of the impacts.

7 EXPERIMENTAL RESULTS

Test results of the small 2.3 kg parafoil outlined in Appendix 2 are shown in Fig. 10 with an away distance of 200 m, cycle distance of 120 m, R of 30 m, and the target at the origin. The parafoil is released 330 m down range and -240 m cross range at an altitude of 610 m above ground. Wind was from 310° with magnitude varying from 4.9 to 6.7 m/s resulting in a wind-to-airspeed ratio of 70 per cent to 98 per cent. Energy management is exited at 211 m, 97 s after release. Homing proceeds until the parafoil is 60 m upwind of the target, 121 s after release, at an altitude of 103 m. The final turn lasts 9.0 s until the FA begins 58 m above ground. The impact occurs 7.4 m away from the target 146 s after release.

8 CONCLUSIONS

A terminal guidance algorithm was developed for parafoil precision placement in high wind-to-airspeed ratios. Using the direct method of calculus of variations and inverse dynamics in a virtual domain, the TPBVP

is reduced to single-parameter optimization problem. The result is an extremely efficient solution that is easily solved in real-time. It was shown, that assuming a constant final turn rate, resulted in an analytic solution that could be used for calculating guidance decisions prior to the final turn. Uncertainty during terminal guidance from wind, sensors, and guidance resulted in the system arriving only approximately at the predicted location. Efficient computation allowed the trajectory to be recomputed during the final turn adding robustness to changing winds and tracking errors. The algorithm was verified using a full 6 DoF parafoil model and Monte Carlo simulations resulting in a circular error probable of 16.8 m. The final test results were presented for a small 2.3 kg system in strong winds where the final error was 7.4 m.

REFERENCES

1 **Benney, R., McGrath, J., McHugh, J., Meloni, A., Noetscher, G., Tavan, S.,** and **Patel, S.** DOD JPADS programs overview and NATO activities. In Proceedings of the 19th AIAA Aerodynamic Decelerator Systems Technology Conference and Seminar, Williamsburg, Virginia, 21–24 May 2007.

2 **Benney, R., Henry, M., Lafond, K., Meloni, A.,** and **Patel, S.** DOD new JPADS programs and NATO activities. In Proceedings of the 20th AIAA Aerodynamic Decelerator Systems Technology Conference and Seminar, Seattle, Washington, 4–7 May 2009.

3 **Benney, R., Meloni, A., Cronk, A.,** and **Tiaden, R.** Precision airdrop technology conference and demonstration. In Proceedings of the 20th AIAA Aerodynamic Decelerator Systems Technology Conference and Seminar, Seattle, Washington, 4–7 May 2009.

4 **Calise, A.** and **Preston, D.** Design of a stability augmentation system for airdrop of autonomous guided parafoils. In Proceedings of the AIAA Guidance, Navigation, and Control Conference and Exhibit, Keystone, Colorado, 21–24 August 2006.

5 **Calise, A.** and **Preston, D.** Approximate correction of guidance commands for winds. In Proceedings of the 20th AIAA Aerodynamic Decelerator Systems Technology Conference and Seminar, Seattle, Washington, 4–7 May 2009.

6 **Gimadieva, T. Z.** Optimal control of a guiding gliding parachute system. *J. Math. Sci.*, 2001, **1**(103), 54–60.

7 **Carter, D., George, S., Hattis, P., McConley, M., Rasmussen, S., Singh, L.,** and **Tavan, S.** Autonomous large parafoil guidance, navigation, and control system design status. In Proceedings of the 19th AIAA Aerodynamic Decelerator Systems Technology Conference and Seminar, Williamsburg, Virginia, 21–24 May 2007.

8 **Slegers, N.** and **Costello, M.** Model predictive control of a parafoil and payload system. *J. Guid. Control Dyn.*, 2005, **4**(28), 816–821.

9 **Slegers, N., Beyer, E.,** and **Costello, M.** Use of dynamic incidence angle for glide slope control of autonomous parafoils. *J. Guid. Control Dyn.*, 2008, **3**(31), 585–596.

10 **Slegers, N.** and **Costello, M.** Aspects of control for a parafoil and payload system. *J. Guid. Control Dyn.*, 2003, **6**(26), 898–905.

11 **Carter, D., Singh, L., Wholey, L., Rasmussen, S., Barrows, T., George, S., McConley, M., Gibson, C., Tavan, S.,** and **Bagdonovich, B.** Band-limited guidance and control of large parafoils. In Proceedings of the 20th AIAA Aerodynamic Decelerator Systems Technology Conference and Seminar, Seattle, Washington, 4–7 May 2009.

12 **Rademacher, B., Lu, P., Strahan, A.,** and **Cerimele, C.** In-flight trajectory planning and guidance for autonomous parafoils. *J. Guid. Control Dyn.*, 2009, **6**(32), 1697–1712.

13 **Yakimenko, O.** Direct method for rapid prototyping of near-optimal aircraft trajectories. *AIAA J. Guid. Control Dyn.*, 2000, **5**(23), 865–875.

14 **Lukacs, J.** and **Yakimenko, O.** Trajectory-shaping guidance for interception of ballistic missiles during the boost phase. *AIAA J. Guid. Control Dyn.*, 2008, **5**(31), 1524–1531.

15 **Forsythe, G. E., Malcolm, M. A.,** and **Moler, C. B.** *Computer methods for mathematical computations*, 1976, pp. 178–187 (Prentice-Hall, Englewood Cliffs, New Jersey).

16 **Natesan, K., Gu, D.,** and **Postlethwaite, I.** Design of linear parameter varying trajectory tracking controllers for an unmanned air vehicle. *Proc. IMechE, Part G: J. Aerospace Engineering*, 2009, **224**(G4), 395–402. DOI: 10.1243/09544100JAERO586.

17 **Ikonen, E.** and **Najim, K.** *Advanced process identification and control*, 2002, pp. 181–197 (Marcel Dekker Inc., New York).

APPENDIX 1

Notation

$\mathbf{A}, \mathbf{B}, \mathbf{C}$	discrete system state space matrices
A, B, C	element of the apparent mass matrix
b	canopy span
$\bar{c}$	canopy mean chord
$\bar{d}$	maximum brake deflection
D_{switch}	distance of the turn initial point with respect to the target
H_P	discrete prediction horizon
$\boldsymbol{i}_I, \boldsymbol{j}_I, \boldsymbol{k}_I$	inertial frame unit vectors
$\boldsymbol{i}_T, \boldsymbol{j}_T, \boldsymbol{k}_T$	target frame unit vectors
k^ψ	turn rate penalty coefficient
K_{turn}	final turn correction gain
L	distance to target along target line
p, q, r	parafoil roll, pitch, and yaw rates in the body frame
P, Q, R	elements of the apparent inertia matrix
$\mathbf{Q}, \mathbf{R}$	positive semi-definite error and control penalty matrices
R	final turn radius
S_{p}	parafoil canopy area
t_{exit}	exit time for final turn
t_{pre}	length of time to apply final turn correction
$T_{\text{app}}, T_{\text{app}}^{\text{des}}$	final approach time and desired final approach time
$T_{\text{app}}^{\text{final}}$	last calculated final approach time

T_{turn}	final turn time	Canopy reference area $S_p (m^2)$	1.1
u, v, w	parafoil velocities expressed in the body frame	Canopy span b (m)	1.35
$\boldsymbol{U}$	discrete optimal control vector	Canopy chord $\bar{c}$ (m)	0.75
V_a	canopy airspeed	Incidence angle Γ (degree)	-12
V_G	parafoil ground speed	Inertia matrix elements (kg m^2)	$I_{xx} = 0.423, I_{yy} = 0.401,$ $I_{zz} = 0.052, I_{xz} = 0.027$
V_h, V_v	parafoil horizontal and vertical speed		
W, W_F	target frame wind speed and ground wind speed	Elements of the apparent mass matrix (kg)	$A = 0.012, B = 0.032,$ $C = 0.423$
x, y, z	parafoil inertial positions in the target frame		
z_{start}	altitude to exit energy management	Elements of the apparent inertia matrix (kg m^2)	$P = 0.054, Q = 0.13,$ $R = 0.0024$
Γ	canopy incidence angle		
δ_a	asymmetric brake deflection	x-distance from mass centre to apparent mass centre x_{BM} (m)	0.05
ε_{final}	final approach efficiency		
λ	speed factor		
τ	virtual time	z-distance from mass centre to apparent mass centre z_{BM} (m)	-1.1
τ_f	virtual time at completion of final turn		
$\bar{\tau}$	virtual time scaled by the final virtual time		
ϕ, θ, ψ	parafoil Euler roll, pitch, and yaw angles	Maximum brake deflection $\bar{d}$ (m)	0.13
ψ^c	commanded final turn angle	Aerodynamic coefficients	$C_{D0} = 0.25, C_{D\alpha2} = 0.12,$ $C_{Y\beta} = 0.23, C_{L0} = 0.091, C_{L\alpha} = 0.90$ $C_{m0} = 0.35, C_{m\alpha} = -0.72, C_{mq} = -1.49$ $C_{l\beta} = -0.036, C_{lp} = -0.84, C_{lr} = -0.082,$ $C_{l\delta a} = -0.0035,$ $C_{n\beta} = -0.0015, C_{np} = -0.082, C_{nr} = -0.27,$ $C_{n\delta a} = 0.0115.$
$\dot{\psi}_{max}$	maximum desired final turn rate		
$\boldsymbol{\psi}^c, \hat{\boldsymbol{\psi}}^c$	desired and estimated output vectors		

APPENDIX 2

Model parameters

System mass m (kg)	2.3
Steady-state aerodynamic velocity V_h (m/s)	6.82